Journal of Applied Fluid Mechanics, Vol. 10, No. 6, pp. 1583-1591, 2017.
Available online at www.jafmonline.net, ISSN 1735-3572, EISSN 1735-3645.
DOI: 10.29252/jafm.10.06.27846

Influence of Smooth Constriction on Microstructure Evolution during Fluid Flow through a Tube

V. H. Ferrer[1], R. Mil-Martínez[1], J. A. Ortega[1] and R. O. Vargas[2†]

[1] *ESIME-Zacatenco, Instituto Polit´ecnico Nacional, U.P. Adolfo López Mateos, Col. Lindavista, Del. Gustavo A. Madero, Ciudad de México, 07738, Mexico.*
[2] *ESIME-Azcapotzalco, Instituto Polit´ecnico Nacional, Av. de las Granjas 682, Col. Santa Catarina, Del. Azcapotzalco, Ciudad de México, 02250, Mexico.*

†*Corresponding Author Email: rvargasa@ipn.mx*

(Received April 4, 2017; accepted June 7, 2017)

ABSTRACT

A numerical solution for axis-symmetrical fluid flow through a smooth constriction using the alternating direction implicit finite volume method and the fractional-step-method is presented. The wall is modelled with a smooth contraction mapped by a sinusoidal function and the flow is supposed to be axis-symmetric. A pressure boundary condition is set at the inlet and the resulting pressure gradient field drives fluid flow which is always in laminar regime. This study presents results for a non-Newtonian fluid using the Ostwaldde Waele constitutive model. Moreover, a transient network representing three different microstructures, immersed in the fluid, is evolved by viscous dissipation and an isothermal process is considered. The time dependent evolution of the transient network is represented by a set of kinetic equations with their respective forward and reversed constants. The numerical predictions show that, at a fixed Reynolds number, the viscous dissipation and the grade of structure restoration or breakage is influenced by constriction severity due to the energy generated during fluid flow. A 50% reduction in transversal section generates secondary flow downstream and vortex shedding, whereas a 10% and 25% constrictions presents a thin boundary layer and no secondary flow near the constricted wall.

Keywords: Generalized Newtonian fluid; Transient network; Finite volume method; Fractional-step method.

Nomenclature

a	pressure at the inlet	Re	Reynolds number
b	initial pressure gradient	R_0	characteristic length
c	average exit velocity	u	velocity in z-direction
C_i	microstructure concentration i = 0,1,2	U	characteristic velocity
D_{max}	maximum diameter	v	velocity vector
D_{min}	minimum diameter		
P	dynamic pressure	v	velocity in r-direction
L	tube length	α	angle of attack
m	consistency parameter	ρ	density
n	power law index	δ	constriction ratio
$r(z)$	variable radius as a function of z coordinate	τ	total stress tensor
		ω_i	microstructure, i = 0,1,2

1. INTRODUCTION

Flow through a contraction or expansion is a classical problem in fluid dynamics and its numerical modelling has a lot of applications such as nozzles (Xiong *et al*. 2015; Allamaprabhu *et al*. 2016), diffuser (Rosa and Pinho 2006; Mariani *et al*. 2010) and throttling valves (Jin *et al*. 2013). Other applications, with both combined geometries, are encountered in Venturi devices (Dong *et al*. 2012; Maqableh *et al*. 2012) and hemodynamics (Ikbal *et al*. 2009; Ponalagusamy and Selvi 2013; Mandal *et al*. 2011). Regardless of the nature of the problem, when a fluid passes a contraction, it experiences a loss in pressure but an increase in kinetic energy. In contrast, when a fluid passes an expansion, it

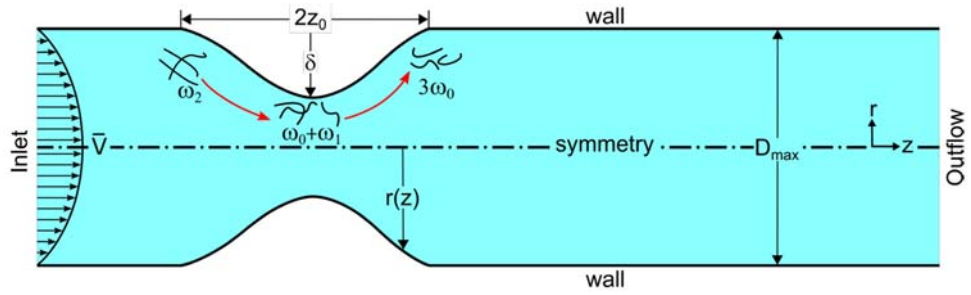

Fig. 1. Schematic of the tube with a smooth constriction showing microstructure breakage due to viscous dissipation.

experiences a loss in kinetic energy but and increase in pressure.

In the early 19th century, Prandtl (1904) noted that fluid flow near a wall is retarded with respect bulk flow and may undergo boundary layer separation. This separated region may occur if a surface undergoes an adverse pressure gradient over a sufficient distance (Sychev 1982). Vortex flow appears in both internal and external flows. Pauley *et al*. (1990) determined that a strong adverse pressure gradient can create periodic vortex shedding from the separation region. In smooth and sudden contractions, the generation of secondary flows and vortex shedding can be avoided by controlling the difference between inlet and outlet pressures, as well as constriction ratio δ :

$$\delta = 1 - \frac{D_{\min}}{D_{\max}} \tag{1}$$

In regard to complex fluids, the phenomena causing secondary flow generation is not much different from that of a Newtonian fluid, but, another interesting arising phenomenon is microstructure evolution. These internal changes make a complex fluid have time and shear-rate dependent behaviour. This behaviour can be approached via constitutive or molecular kinetic models. For instance, Binding *et al*. (2006) numerically determined the flow through contraction and expansion of an Oldroyd-B fluid; Mu *et al*. (2014) carried out simulations using FENE-P model for flow through a sudden contraction; Siddiqui *et al*. (2016) analyzed theoretically the steady flow of a second grade fluid through a constricted tube.

The goal of this work is to present a simple model for microstructure distribution. The flow of a generalized Newtonian fluid through a constricted tube is treated numerically, and a transient network is added to evaluate the microstructure evolution which depends on the thermal energy generated during fluid flow. This thermal energy is due to viscous dissipation and it is supposed to be wasted by microstructure breakage. Numerical predictions are compared and discussed in detail with available published in literature for the flow through a stenosed vessel. This model can be used for blood flow predictions regarding structure kinetics. Furthermore, it can be used as an analysis or diagnostic tool to interpret complex fluids in different geometries subjected to different boundary and initial conditions.

2. MATHEMATICAL MODELLING

In this sections is treated all about governing equations, constitutive model, microstate kinetic equations, boundary conditions and numerical procedure.

Consider the flow of a generalized Newtonian fluid through a constricted tube with some microstructures diluted in it, as depicted in Fig. 1. In this case, three constricted ratios are selected to evaluate how microstructure evolves by the action of viscous dissipation and this thermal energy is assumed to be totally consumed by the disentanglement process. These microstructural changes are analyzed with a simplified version of Rincón *et al*. (2005), model where the microstate configuration determines an averaged extensibility linked to a spring force law. Here, the purpose is just to determine the microstructure distribution without considering how these ones affect fluid properties. In addition, it is analyzed the boundary geometry influence on the velocity field.

2.1 Governing Equations

Consider two-dimensional flow in a circular constricted tube with constant density ρ and strain rate dependent viscosity η (**d**). Here **d** denotes the symmetric part of the velocity gradient tensor. For dimensional analysis the following dimensionless variables are defined:

$$x = \frac{x^*}{R_0},\ v = \frac{v^*}{U},\ t = \frac{t^* U}{R_0},\ P = \frac{P^*}{\rho U^2}, \tag{2}$$

where x and v are the position and the velocity vectors. The scalar quantities t, p, R_0 and U are time, pressure, characteristic length and mean inlet velocity vector, respectively. In this case $R_0 = 0.5 D_{\max}$.

Since the fluid is assumed to be incompressible, the continuity equation is expressed as follows

$$\nabla \cdot \mathbf{v} = 0, \tag{3}$$

and momentum transfer is defined by the Cauchy equation of motion:

$$\frac{\partial v}{\partial t} + \mathbf{v} \cdot \nabla v = -\nabla p - \frac{1}{\mathrm{Re}} \nabla \cdot \boldsymbol{\tau}, \tag{4}$$

where τ is the total stress tensor. This stress tensor takes the form of a generalized Newtonian fluid with no temperature dependence.

$$\tau = -(\frac{1}{2}\mathbf{d} : \mathbf{d})^{\frac{n-1}{2}} \mathbf{d}. \tag{5}$$

The Reynolds number (*Re*) is defined as:

$$\mathrm{Re} = \frac{\rho R_0^n}{m U^{n-2}} \tag{6}$$

where *m* is the consistency parameter and n is the power law index.

2.2 Microstructure Kinetic Equations

Network models are capable to predict fluid flow phenomena for concentrated solutions and melts by considering temporal physical interactions or junctions between structures (Bird *et al*. 1987). In a classical sense, a transient network describes polymer-polymer interactions. But in this case, it can be thought of as general isolated microstructures capable of changing their actual configuration. Under the current hypothesis, the microstructures are sufficiently separated from each other such that the fluid is a very dilute solution.

When the fluid is at rest, all diluted microstructures are in ω_2 microstate configuration. By action of fluid flow and the inherent viscous dissipation, the required internal thermal energy is produced and is used by the system to break original microstructures into simpler microstructures, i.e., ω_0 and ω_1 (see Fig. 1). Instead of tracking each microstructure and their current microstate, it is a better idea to compute their concentration C_i , where i = 0, 1, 2 and this subindex indicates which microstate is being represented $(\omega_0,\ \omega_1$ or $\omega_2)$.

The following set of kinetic equations are based on a transient network model that can be found in Rincón *et al*. (2005)

$$\frac{dC_0}{dt} = B\,\tau : d\,(C_1) - A\,(C_0^2), \tag{7}$$

$$\frac{dC_1}{dt} = B\,\tau : d\,(C_2^2 - C_1) - A\,(C_1^3 - C_0^2), \tag{8}$$

$$\frac{dC_2}{dt} = A\,(C_1^3) - B\,\tau : d\,(C_2^2). \tag{9}$$

These equations computes microstructure concentrations and are used just to predict their variation with time and spatial distribution. The parameters *A* and *B* are the forward and reverse rate constants, respectively. Here, A is related to the exponential function which models structure build-up, and *B* is related to internal friction dissipation, allowing structure breakage.

2.3 Initial and Boundary Conditions

The problem is approximated as an axis-symmetrical flow through a circular tube. The boundaries includes a solid wall at the top, an inlet, an outlet and a line of symmetry, as shown in Fig. 1.

The initial conditions (t = 0) for the momentum equation are:

$$\begin{aligned} u &= 2(1 - r^2) \\ v &= ru\frac{dR}{dz} \\ p &= a + \frac{\Delta p}{L} z\,. \end{aligned} \tag{10}$$

where the function $R(z)$ defines the geometry of the constricted tube as defined in Ikbal *et al*.(2009)

$$R(z) = R_0 - \frac{\delta}{2}\left[1 + \cos\left(\pi \frac{z - z_1}{z_0}\right)\right], \tag{11}$$

when there is no constriction, $\mathrm{R}(\mathrm{z}) = \mathrm{R}_0$ and δ is the constriction ratio. The value of z_1 defines the constriction centre with respect z coordinate. The parameters a and $\Delta p / L$ represent the pressure at the inlet and initial pressure gradient per unit length. L is the length of the tube section under analysis.

The initial microstate corresponds to one in which ω_2 structures are present all over the domain and there is no probability to find ω_0 and ω_1 structures. According to Rincón *et al*. (2005), ω_0 is made of one segment, ω_1 of two segments and ω_2 of three segments. Scaling microstructure concentrations, using the maximum number of ω_0 structures that can be present in the system, their limiting value per control volume are determined by the inverse of individual structures of their respective microstate, that is, $\mathrm{C}_0 = 1$, $\mathrm{C}_1 = 1/2$ and $\mathrm{C}_2 = 1/3$. For initial condition

$$C_0 = C_1 = 0;\ C_2 = \frac{1}{3} \quad for\ t \le 0. \tag{12}$$

A pressure inlet boundary condition is set, thus, velocities u and v are unknown, except at $t = 0$

$$p = 0 \quad at \quad z = 0 \tag{13}$$

A convective boundary condition is set at the outflow, which allows the propagating vortex structure to exit the domain with minimum distortion

$$\frac{\partial u}{\partial t} = c\frac{\partial u}{\partial z},\ \frac{\partial v}{\partial t} = c\frac{\partial v}{\partial z} \quad at \quad z = L, \tag{14}$$

where c can be either the propagation speed of vortices or the average exit velocity (Pauley *et al*. 1990).

At the top wall, a no-slip condition is prescribed

$$u = 0, \quad v = 0 \quad at \quad r = R(z). \tag{15}$$

At the symmetry, a Neummann boundary condition is used for u and a Dirichlet one for v:

$$\frac{\partial u}{\partial r} = 0, \quad v = 0 \quad at \quad r = 0. \tag{16}$$

3. Method of Solution

3.1 Numerical Procedure

A semi-implicit second-order-accurate alternating direction implicit (ADI) finite-volume method was used to solve Eq. (4) (Singh and You 2011). Once the integral approach of the finite volume method is performed the ADI factorization proposed by Douglas and Gunn (1964) is applied. Then, the resulting equations are solved by means of a Newton-iterative method and finally the fractional-step method is employed to update u, v and p to their actual values (Kim and Moin 1985). The strain rate dependent viscosity is computed using previous time-step information or initial conditions, whatever the case. After computing the velocity field and pressure distribution, the viscous dissipation is calculated and its values is passed to the discrete kinetic equations, which correspond to Eqs. (7) to (9). This system was solved with a fourth order Runge-Kutta method.

The dimensionless length of computational domain is 50 and the dimensionless maximum diameter is 2, implying that $R_0 = 1$. The time-step size for all simulations is 1×10^{-3}. The initial pressure gradient in z direction is -0.01.

3.2 Grid Independence Test

A grid independence test was conducted using four different grid sizes of 251 × 21, 351 × 31, 501 × 41 and 701 × 61 with a Reynolds number of 200 and for a Newtonian fluid. The constriction ratio is 0.5. It was observed that a further refinement of grids from 501×41 to 701×61 do not provide a significant improvement over velocity and pressure calculations. Based on this information, the 501 × 41 grid size was selected to perform simulations.

3.3 Validation of Numerical Formulation

In order to assess the reliability o the numerical algorithm, this is compared with a finite difference solution developed by Ikbal *et al.* (2009) for a shear-thinning fluid in a pulsatile stenosed blood flow with $\delta = 0.276$. Fig. 2 depicts the finite difference and present finite volume (FVM) solutions for a non-Newtonian fluid with a power law index $n = 0.639$. The comparison between u and v velocity profiles with a Reynolds number of 300 is shown in Fig. 2(a). In this case the profiles are similar but do not match at all. Volumetric flow rate for a shear-thinning fluid with a power law index of 0.639 and a Reynolds number of 1000 is compared in Fig. 2(b) and Fig. 2(c). In general, contours are in agreement but near the inlet they have appreciable differences. To ensure code validity, Ikbal numerical finite difference procedure was reproduced and showed the same performance as the current finite volume method procedure. It is important to state that the phase angle, used by Ikbal *et al.* is unknown and was estimated.

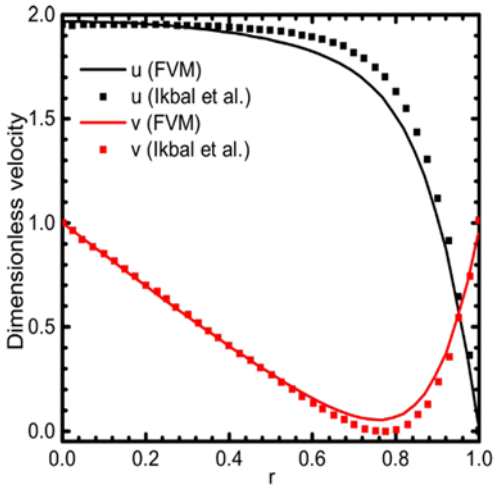

Fig. 2. (a) Velocity profiles at Re=300, z=14 and t=50. (b) and (c) volumetric flow contours computed in the present work and by Ikbal *et al.*, respectively; Re=1000, t=1000 and n=0.639.

4. Results and Discussion

Results for three different constriction ratios are treated in this section, $\delta = 0.10$, 0.25 and 0.50. The fluid has a shear-thinning behaviour and its power law index is $n = 0.639$. For the system of kinetic equations two couples of forward and reversed kinetic constants have been selected. For a weakly structured network $A = 0.01$ and $B = 0.1$. For a highly structured network $A = 0.1$ and $B = 0.01$.

4.1 Fluid Flow Phenomena

Figure 3 shows fluid flow information for t = 500. In this figure, it can be noticed that for δ = 0.1 and δ= 0.25 do not exist separation and flow instabilities, but for δ= 0.5, secondary flows and vortex shedding occurs. When flow separation appears, no reattachment is observed since the outflow boundary conditions allows nonfully developed velocity profiles. Fig. 3(a) shows that velocity magnitudes results to be proportional before and after the constriction centerline at z = 15 for δ= 0.1. Fig. 3(b) reveals the existence of a wider region of low velocity near the wall after the constriction centerline, which is a result of having increased the constriction ratio.

Although in this work, it was considered a symmetric flow, it is more probable, that for certain high critical Reynolds numbers, instabilities make fluid flow be asymmetric with respect the *z-axis*. In this case, it is not clear if vortices start vanishing due to a natural subsequent reattachment or because the system is trying to comply the imposed symmetric boundary

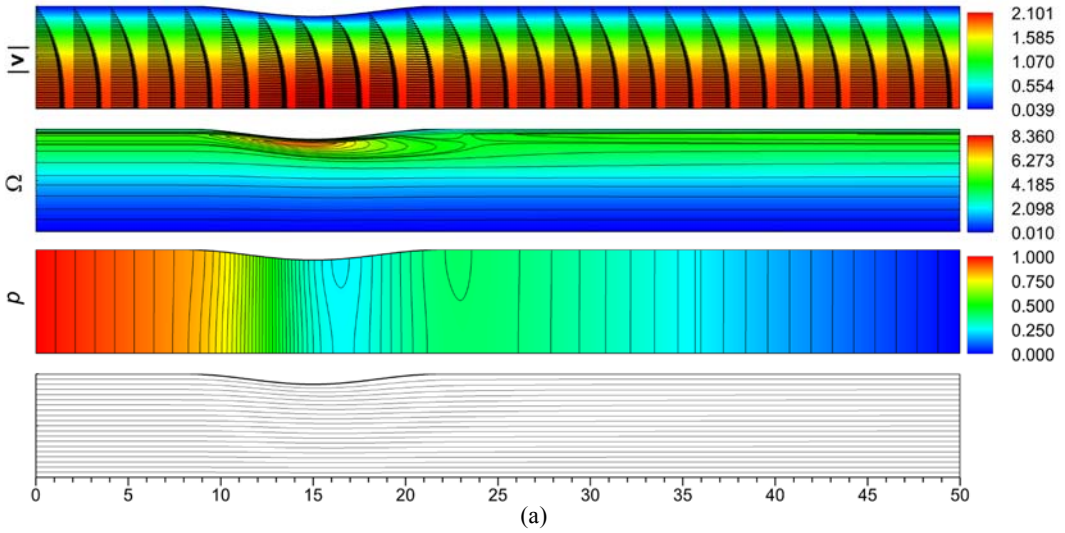

(a)

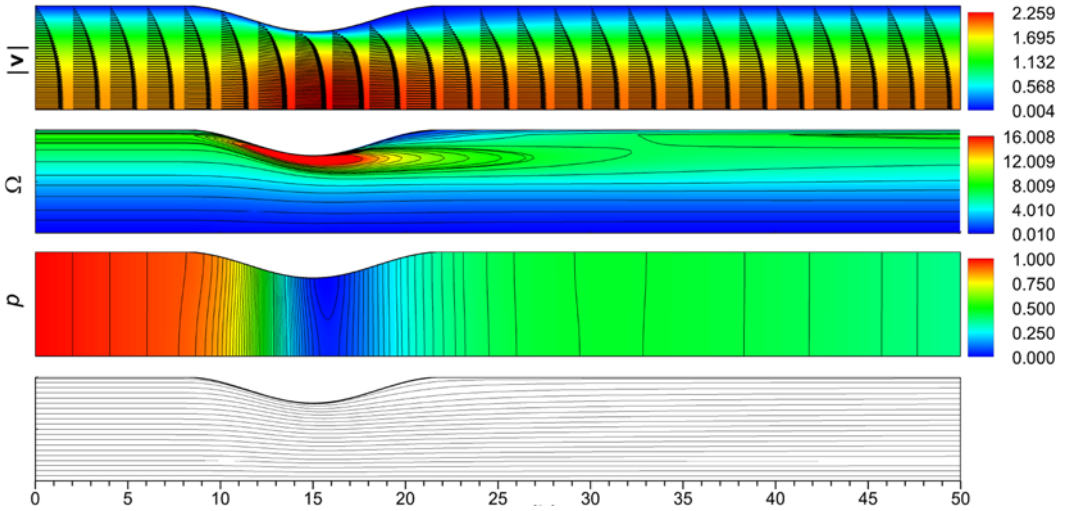

(b)

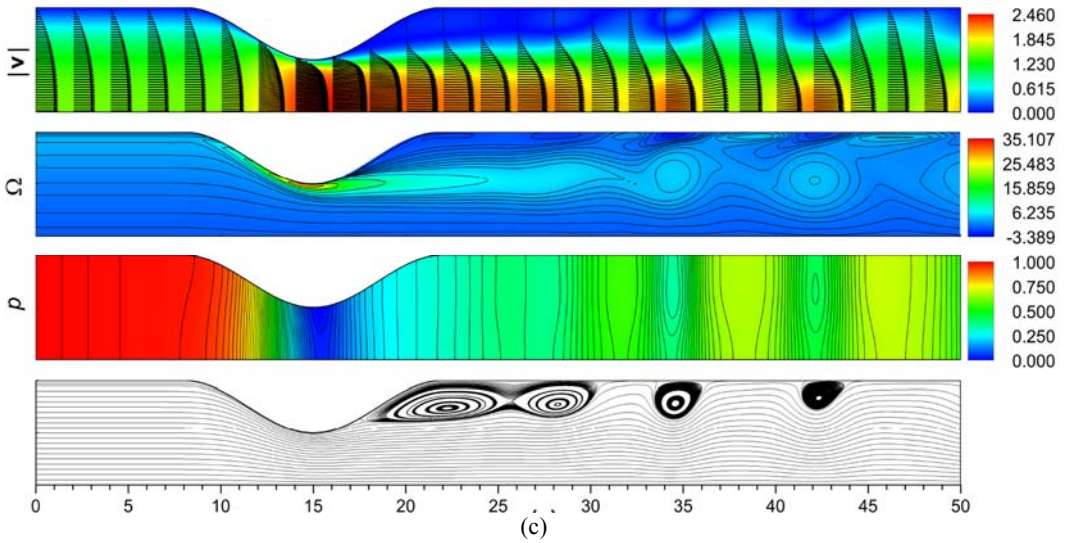

(c)

Fig. 3. From top to bottom: Velocity magnitude and profiles; vorticity Ω, normalized pressure *p*, and streamlines. Constriction ratio (a) δ= 0.1, (b) δ =0.25, (c) δ =0.50, *Re*=500 and *t* = 500.

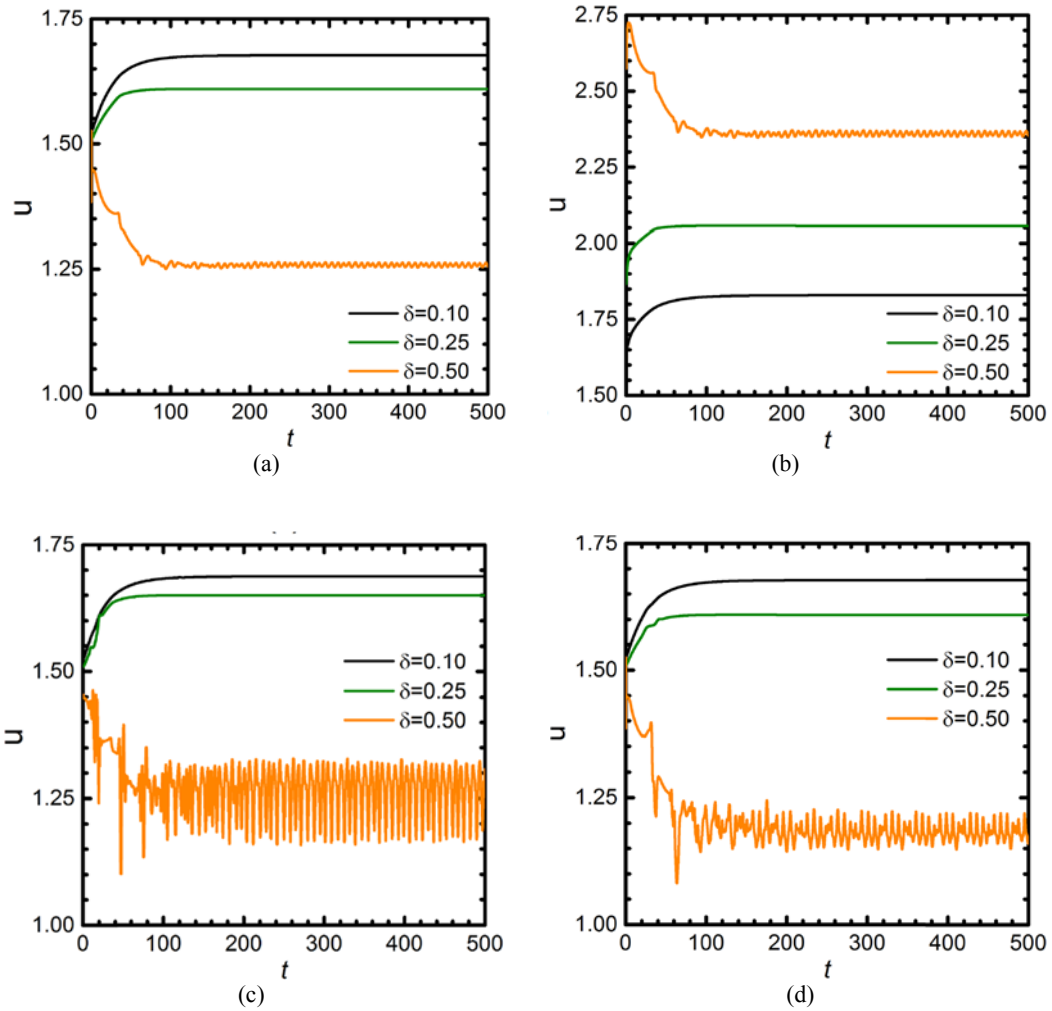

Fig. 4. Time evolution of *u* velocity at dierent longitudinal locations and at *r* = 0.5. (a) At the inlet. (b) At the constriction center. (c) After constriction. (d) At the outlet.

condition. Streamlines in Fig. 3, imply that the critical Reynolds number of flow separation or bifurcation is modified by the constriction ratio. This critical values is also modified by the width, in z direction, of the constriction (Boghosian and Cassel 2013).

Table 1 shows average velocities over area for three different positions and each constriction ratio. It can be notice that mass is conserved in terms of the product between averaged velocity and cross sectional area. The averaged velocity out of constricted region tends to be lower for higher constriction ratios. This is caused because pressure was set as a boundary condition but velocity is unknown. For the three constriction cases the inlet pressure is the same and a reduction in velocity (when increasing the constriction ratio) at the inlet ensures mass conservation. Attempting to specify a fixed velocity profile and pressure, at once, lead to physically impossible solutions and numerical divergence at high Reynolds numbers. The fluid, for δ= 0.10, passes through the constriction with an increase of 23% in kinetic energy; for δ = 0.25 is 78%, and for δ = 0.50 is 296%. Vorticity is higher near the constricted wall and for the first half, from left to right. Approximately, at z = 15 its value tends to decrease and have negative values near the wall. The fluid motion is always rotational in counter clockwise direction, except for δ = 0.5, where vorticity has negative values in the recirculation region and shed vortices. These vortices are split from the main vortex located at the second half of the constriction.

Table 1 Averaged velocity

	Position		
δ	z = 0	z = 15	z = 25
0.10	1.44	1.60	1.44
0.25	1.38	1.84	1.38
0.50	1.08	2.15	1.08

From Fig. 4, it is evident that only when δ = 0.5, there exist fluctuations in u velocity due to vortex shedding. The other two values of δ do not exhibit this behaviour. The velocities are measured at the tube symmetry (r = 0). Fluctuations are weaker at the

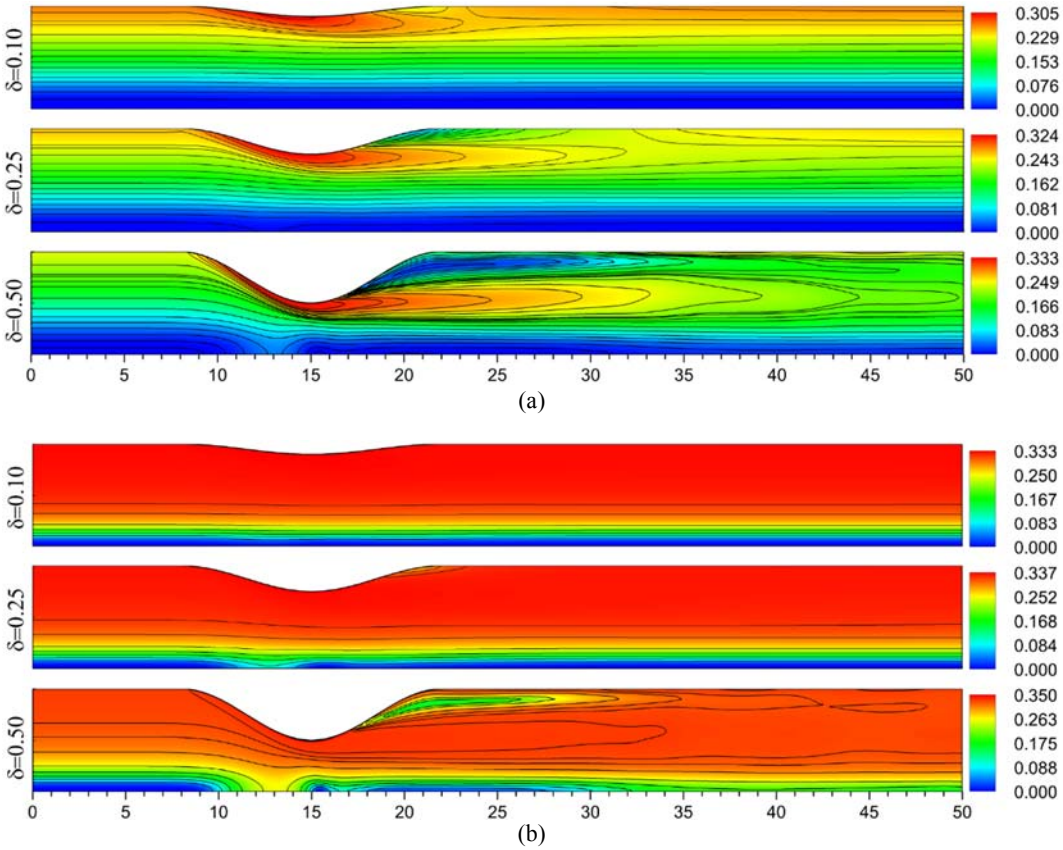

Fig. 5. Microstate concentration C_0 at three dierent constriction ratios. (a) For a highly structured network. (b) For a weakly structured network.

inlet and constriction center, and stronger where vortex splitting occurs. At the outlet, their amplitude is diminished but still higher than at the two first aforementioned positions. The dominant Strouhal number is S_t = 0.1333. This number is defined as $S_t = fR_0 / U$, and relates the characteristic oscillation frequency f to the inverse of the flow residence time, $\mathrm{U} / \mathrm{R}_0$.

The computed pressure is normalized and recast with the following expression:

$$p = \frac{p - p_{\min}}{p_{\max} - p_{\min}} \tag{17}$$

All cases show a decrease in pressure in the constricted zone, and this decrement is proportional to the increase in kinetic energy. In Figs. 3(a) and 3(b) the pressure is gradually reduced at the constricted region. Then, the fluid leaves this region and pressure is increase due to the expansion. Far downstream, the pressure decreases again. When the constriction ratio is changed from $\delta = 0.1$ to $\delta = 0.25$, the same behaviour is observed, except that the lowest pressure values are located at the outlet in the first case, whereas they are located in the constriction for the second case. Pressure distribution, in Fig. 3(c), give rise to adverse pressure gradients which help to maintain vortical structures.

4.2 Microstructure Evolution

Rincón *et al.* (2005) considered five different microstructures and suggested that these are the basic microstates. Although there could be other individual structures describing the same microstate, but, those with lower energy are preferred. As an extension to this work, Manero *et al.* (2015) considered individual structure self-entanglement, which increase the number of microstructures to be modeled. Both models can predict shear banding in complex fluids. In the current work, it is computed the spatial distribution of three microstructures without considering their effect in fluid properties.

Figure 5 and Fig. 6 depict microstructure concentration results for highly and weakly structured networks. Concentration distributions of ω_0 are shown in Fig. 5 for three different constriction ratios. Near the line of symmetry, low viscous dissipation does not allow structure breakage, thus, C_0 is approximately zero. The higher microstructure destruction occurs near the constricted wall for all cases. This fact is more noticeable for highly structured networks.

A comparison between Fig. 5(a) with Fig. 5(b), makes it evident that for weakly structured networks the concentrations are more uniformly distributed.

An Increase in constriction ratio, reduces uniform distribution of single element structures due to low viscous dissipation in the regions of lower vorticity. In parabolic-like velocity profiles, the viscous dissipation always is lower near the axis of symmetry that near the walls. Referring to viscous dissipation as low or high, is relative to the necessary energy promoting structure breakage. It is very interesting that the fluid reach a periodic equilibrium state, but microstructures do not reach any equilibrium at the given energy dissipation rate (Fig. 6). The only microstructure reaching an equilibrium concentration is ω_1 for a weakly structured network and a constriction ratio of 0.5, as depicted in Fig. 6b. Microstructure concentration results for $\delta = 0.1$ are omitted since there is no remarkable difference between them and those for $\delta = 0.25$. This information suggests that other structures need more time to reach equilibrium, and this time depends on wether the network is weakly or highly structured. Equilibrium concentrations can be locally obtained at discrete points of the domain, but their global average do not reflect this, at least, up to a time t=500.

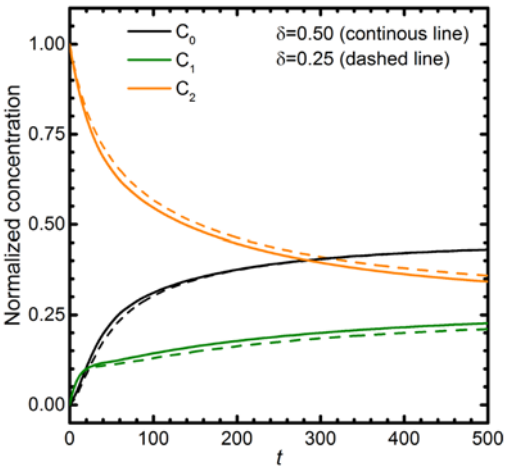

(a)

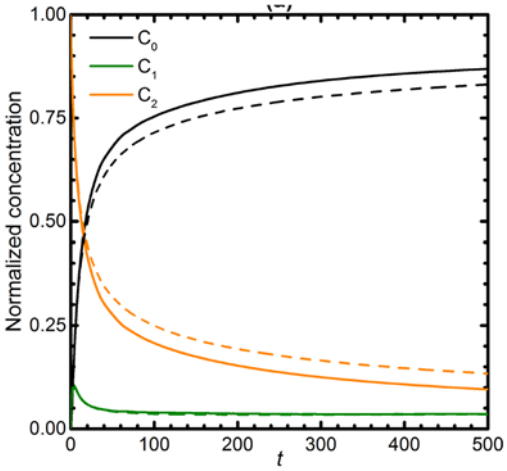

(b)

Fig. 6. Time evolution of normalized microstructure concentrations for a constriction ratio $\delta = 0.5$. (a) For a highly structured network. (b) For a weakly structured network.

The present work only considers microstructure evolution. In this case the fluid is non-Newtonian and its viscosity depends on shear rate but not time. The issue is when microstructure concentrations become sufficiently large, such that they are capable of modifying fluid properties. Structure breakage will result in thixotropy and structure build-up in anti-thixotropy (Ferrer *et al*. 2017; Mewis and Wagner 2009; Quemada 1999).

5. CONCLUSIONS

A 2-D numerical model has been presented to addressed axis-symmetrical fluid flow through a constriction of a generalized Newtonian fluid with microstructures. The selected power law index is n = 0.639. The method of solution is based on an alternating direction implicit finite volume method for spatial integration and the fractional-step method for time integration. The extension of this model to 3-D and none-symmetric cases is straightforward. Blood Flow numerical model through a stenosed vessel was compared with numerical results from the literature, and a good match has been found in terms of the volumetric flow rate and velocity profiles. The influences of the constriction ratio on the microstructure distribution, at a given Reynolds number, have been assessed. This study showed that reducing the transversal area, increase the microstructure breakage in the regions of higher vorticity. Two types of behaviour were selected for microstructures; the first corresponds to weakly structured networks and is represented by kinetic constants A less than B, and the second one by A greater than B. The microstructure distribution for a weakly structure network showed to be more homogeneous than for a highly structure network.

The procedure presented in this paper, would be used to model a complex fluid taking into account microstate kinetics coupled with a stochastic or constitutive model, for instance, micellar or flocculant systems. Another application would be in blood flow considering the kinetics of red and white cells and/or low and high density lipoproteins.

ACKNOWLEDGMENTS

First author would like to acknowledge the financial support from the National Council of Science and Technology (CONACyT) of México. ROV appreciate support from project SIP-IPN 20171482.

REFERENCES

Allamaprabhu, Y., B. N. Raghunandan and J. A. Moríñigo (2016). Numerical prediction of nozzle flow separation: Issue of turbulence modeling. *Aerospace Science and Technology 50*, 31–43.

Binding, D. M., P. M. Phillips and T. N. Phillips (2006). Contraction/expansion flows: The pressure drop and related issues. *Journal of Non-Newtonian Fluid Mechanics 137* (1-3), 31–38.

Bird, R. B., R. C. Armstrong and O. Hassager (1987).

Dynamics of polymeric liquids, Fluid mechanics, Volume 2. New York: John Wiley and Sons.

Boghosian, M. E. and K. W. Cassel (2013). A pressure–gradient mechanism for vortex shedding in constricted channels. *Physics of Fluids 25* (12), 123603.

Dong, C., J. Zhu, X. Wu and C. F. Miller (2012). Aeration efficiency influenced by venturi aerator arrangement, liquid flow rate and depth of di using pipes. *Environmental Technology 33* (11), 1289–1298.

Douglas, J. J. and J. E. Gunn (1964). A general formulation of alternating direction methods. *Numerische Mathematik 6*(1), 428–453.

Ferrer, V. H., A. Gómez, J. A. Ortega, O. Manero, E. Rincón, F. López Serrano and R. O. Vargas (2017). Modeling of complex fluids using micro-macro approach with transient network dynamics. *Rheologica Acta 56*(5), 445–459.

Ikbal, M. A., S. Chakravarty, K. K. L. Wong, J. Mazumdar and P. K. Mandal (2009). Unsteady response of non-newtonian blood flow through a stenosed artery in magnetic field. *Journal of Computational and Applied Mathematics 230*(1), 243–259.

Jin, Z., L. Wei, L. Chen, J. Qian and M. Zhang (2013). Numerical simulation and structure improvement of double throttling in a high parameter pressure reducing valve. *Journal of Zhejiang University SCIENCE A 14* (2), 137–146.

Kim, J. and P. Moin (1985). Application of a fractional–step method to incompressible Navier–Stokes equations. *Journal of Computational Physics 59* (2), 308–323.

Mandal, D. K., N. K. Manna, and S. Chakrabarti (2011). Influence of primary stenosis on secondary one and vice versa in case of double stenoses. *Journal of Applied Fluid Mechanics 4* (4), 31–42.

Manero, O., J. E. Puig, F. Bautista and J. P. Garcia-Sandoval (2015). Nonlinear viscoelasticity of complex fluids: *A kinetic network model. Rheologica Acta 54*(1), 53–67.

Maqableh, A. M., S. A. Ammourah, A. Khadrawi, M. A. Al Nimr and A. C. Benim (2012). Hydrodynamics behaviour of a fluid flow in microventuri. *Canadian Journal of Physics 90*(1), 83–89.

Mariani, V. C., A. T. Prata and C. Deschamps (2010). Numerical analysis of fluid flow through radial diffusers in the presence of a chamfer in the feeding orifice with a mixed eulerianlagrangian method. *Computers and Fluids 39*(9), 1672–1684.

Mewis, J. and N. J. Wagner (2009). Thixotropy. *Advances in Colloid and Interface Science 147–148*, 214–227.

Mu, Y., G. Zhao, A. Chen, G. Dong and S. Li (2014). Finite element simulation of three-dimensional viscoelastic planar contraction flow with multi-mode fenep constitutive model. *Polymer Bulletin 71*(12), 3131–3150.

Pauley, L. L., P. Moin and W. C. Reynolds (1990). The structure of two-dimensional separation. *Journal of Fluid Mechanics 220*, 397–411.

Ponalagusamy, R. and R. T. Selvi (2013). Blood flow in stenosed arteries with radially variable viscosity, peripheral plasma layer thickness and magnetic field. *Meccanica 48*(10), 2427–2438.

Prandtl, L. (1904). *Uber flüssigkeitsbewegung bei sehr kleiner reibung*. Proceedings of the Institution of Mechanical Engineers 452, 484–491.

Quemada, D. (1999). Rheological modelling of complex fluids:iv: Thixotropic and thixoelastic behaviour. startup and stress relaxation, creep tests and hysteresis cycles. *The European Physical Journal Applied Physics 5*(2), 191–207.

Rincón, E., A. E. Chávez, R. Herrera and O. Manero (2005). Rheological modelling of complex fluids: A transient network model with microstate. *Journal of non-Newtonian Fluid Mechanics 131*, 64–77.

Rosa, S. and F. T. Pinho (2006). Pressure drop coeffient of laminar newtonian flow in axisymmetric diusers. International *Journal of Heat and Fluid Flow 27*(2), 319–328.

Siddiqui, A. M., N. Z. Khan, M. A. Rana and T. Haroon (2016). Flow of a second grade fluid through constricted tube using integral method. *Journal of Applied Fluid Mechanics 9*(6), 2803–2812.

Singh, S. and D. You (2011). A multiblock ADI finite-volume method for incompressible Navier–Stokes equations in complex geometries. *Journal of Computational Physics 230*(19), 7400–7417.

Sychev, V. V. (1982). Asymptotic theory of separation flows. *Fluid Dynamics 17*(2), 179–188.

Xiong, Y., M. S. Cha and S. H. Chung (2015). *Fuel density effect on near nozzle flow field in small laminar coflow diusion flames*. In Proceedings of the Combustion Institute.